The Cryosphere
Discussions

Open Access

EGU

Mapping snow depth over lake ice in Canada's sub-arctic using ground-penetrating radar

Alicia F. Pouw[1,2], Homa Kheyrollah Pour[1,2], Alex MacLean[1,2]

[1]Remote Sensing of Environmental Change (ReSEC) Research Group Department of Geography and Environmental Studies,
Wilfrid Laurier University, Waterloo, N2L 3C5, Canada

[2]Cold regions Research Centre, Wilfrid Laurier University, Waterloo, N2L 3C5, Canada

Correspondence to: Alicia F. Pouw (apouw@wlu.ca)

Abstract

Ice thickness across lake ice is influenced mainly by the presence of snow and its distribution, as it directly impacts the rate of lake ice growth. The spatial distribution of snow depth over lake ice varies and is driven by wind redistribution and snowpack metamorphism, creating variability in the lake ice thickness. The accuracy and consistency of snow depth measurement data on lake ice are challenging and sparse to obtain. However, high spatial resolution lake snow depth observations are necessary for the next generation of thermodynamic lake ice models. Such information is required to improve the knowledge and understanding of snow depth distribution over lake ice. This study maps snow depth distribution over lake ice using ground-penetrating radar (GPR) two-way travel-time (TWT) with ~9 cm spatial resolution along transects totalling ~44 km over four freshwater lakes in Canada's sub-arctic. The accuracy of the snow depth retrieval is assessed using in situ snow depth observations (n =2,430). On average, the snow depth derived from GPR TWTs for the early winter season is estimated with a root mean square error (RMSE) of 1.58 cm and a mean bias error of -0.01 cm. For the late winter season on a deeper snowpack, the accuracy is estimated with RMSE of 2.86 cm and a mean bias error of 0.41 cm. The GPR-derived snow depths are interpolated to create 1 m spatial resolution snow depth maps. Overall, this study improved lake snow depth retrieval accuracy and introduced a fast and efficient method to obtain high spatial resolution snow depth information, which is essential for the lake ice modelling community.

1 Introduction

The distribution of snow depth over lake ice affects the formation and thickness of ice over the entire lake. While snowfall can advance the onset of lake freeze-up, once the ice has formed, the snow accumulation hinders the ice growth in the water column (Adams, 1976a). Snow present on lake ice acts as an insulative barrier due to the lower thermal conductivity of snow than that of ice and, therefore, affects the heat released from the water column to the atmosphere. This process slows the growth rate of congelation ice (or black ice) (Brown and Duguay, 2010; Leppäranta, 2015). While snow on lake ice can inhibit ice growth,

snow can also affect the timing of melt and the ice-free season. The albedo of the snow surface reflects incoming solar radiation
30   and can lead to a longer ice-on season (Jensen et al., 2007; Brown and Duguay, 2011; Robinson et al., 2021). Additionally, snow produces ice growth, as snow ice, if the snow on the ice surface encounters water, forming slush, and then freezing (Leppäranta, 1983). This process can occur through the upwelling of water through cracks, precipitation falling as rain, or heavy snow causing the depression of ice below the water level.

Snow and lake ice are sensitive to a change in air temperature. As warming is occurring in Northern Canada at twice the global
35   rate and is expected to continue to increase (Zhang et al., 2019), a change in the surface-atmosphere energy balance will directly affect snow and lake ice conditions (Brown and Duguay, 2010). Changes are causing a shift in ice-on season duration (Magnuson et al., 2000; Benson et al., 2011) and ice thickness (Kholoptsev et al., 2021). Northern communities rely on lake ice for cultural and recreational use and as a source of transportation through ice roads (Knoll et al., 2019). Ice roads allow travel to neighbouring communities and alternative access to goods and supplies (instead of transport via airplane). With
40   warming projected to increase, it can be expected that the safety of ice roads and operational duration will be affected (Stephenson et al., 2011; Mullan et al., 2021). As the presence of snow over lake ice directly affects ice thickness, measuring snow depth on lake ice is crucial for lake modelling and ice thickness estimation on a regional scale. Previous studies show that accurate snow depth observations over lake ice can significantly improve the thermodynamic lake ice models (Kheyrollah Pour et al., 2017).

45   Improving snow depth observations and retrieving an accurate higher spatial resolution snow depth is essential for hydrological and lake ice studies (Kheyrollah Pour et al., 2017; Marsh et al., 2020). Daily snow depths are reported across Canada using instruments, such as a manual ruler or a sonic sensor, at weather stations located on land (Brown et al., 2021). However, the depth of snow on land does not compare to snow over lake ice (Sturm & Liston, 2003). Snow depth over lake ice is ~ 30 % less than that over land (Gunn et al., 2015; Kheyrollah Pour et al., 2017), such that incorporating land-based snow observations
50   into a thermodynamic lake ice model would negatively bias the ice thickness estimations. The distribution of snow over lake ice is affected more significantly by wind due to the open nature of lakes and the lack of vegetation catchments, which also create a heterogeneous snow surface across the lake ice (Adams, 1976a).

Currently, retrieving accurate snow depth observations over lake ice and mapping the spatial distribution and heterogeneity of snow over ice is challenging because of the limited support of point measurements using contemporary methods (Sturm and
55   Holmgren, 2018). Due to the limited spatial coverage that current methods pose; it is not logistically feasible to measure the snow depth on lake-wide scales. Furthermore, recent advancements have utilized Structure from Motion (SfM) from remotely piloted aircraft system (RPAS) acquisitions to map snow depth over land (i.e., Harder et al., 2016; 2020; Walker et al., 2020; King et al., 2022). This technique is limited in representing the lake ice surface elevation because the ice surface is rarely exposed prior to snow accumulation, and the accumulation of snow, which submerges the ice, invalidates the elevation baseline
60   (Adams, 1976b). A freeboard correction compensates for the change in ice surface elevation to the open water surface; however, this method requires prior information on the snowpack and ice thickness (Gunn et al., 2021a). Ground-penetrating radar (GPR) is one technique that can simultaneously estimate snow depth and ice thickness to be applied within the freeboard

2

correction. GPR systems transmit an electromagnetic (EM) wave and record the measured amplitude as a function of two-way travel-time (TWT) as the signal travels from the transmitting antenna, through a medium and reflects back to the receiving

65   antenna at each interface. Although, GPR is a recognized tool for measuring the spatio-temporal patterns of deep snow over land, sea ice, and glacial firn (i.e.,Webb, 2017; Webb et al., 2018; McGrath et al., 2019, 2022; Meehan et al., 2020; 2021; Pfaffhuber et al., 2017), it still requires observation of dry snow density (or snow depth and the radar travel-time for calibration) to derive snow depth from the GPR TWT (Marshall et al., 2005). Over lake ice, GPR is commonly used to retrieve ice thickness (i.e., Barrette, 2011; Gunn et al., 2021a; 2021b); however, lake snow depth retrieval using GPR is challenging due to the GPR

70   signal attenuations, as well as the shallow snow-ice interface. These challenges are mitigated through additional signal processing of the radargrams, as presented in this work.

Our goal is to improve the knowledge and understanding of snow depth distribution over lake ice. We utilize extensive GPR two-way travel-time (TWT) observations and in-situ observations of lake snow depth and density to complete the following objectives: (1) Improve the retrieval of lake snow depth observations by adapting a fully automated snow processing algorithm

75   for lake ice using GPR TWTs, (2) validate the snow-depth retrieval algorithm using in situ observations, and (3) map the distribution of snow depth spatially over lakes. The outcome will increase of lake snow depth data availability which benefits the hydrological and lake ice modelling communities.

2 Study area

In this study, GPR is used to derive and map snow depth over lake ice on four freshwater lakes located north of Yellowknife

80   NWT during the early and late winter season, such as Landing Lake (62.5587 °N, 114.4103 °W), Finger Lake (62.5750 °N, 114.3587 °W), Long Lake (62.4772 °N, 114.4422 °W), and Vee Lake (62.5555°N, 114.3502 °W) shown in Figure 1. All four lakes are located within the North Slave region. These lakes are generally covered by ice from October to April. The four lakes are close in proximity to one another but vary in shape and size (Table 1). It is expected that the wind fetch and shoreline vegetation affect the snow distribution on these lakes differently. This study uses data collected on areas within the four lakes,

85   as identified in Figure 1b, covering regions along the shoreline, as well as open areas.

Data collection for this study took place during the 2021-2022 early winter season (between December 7th to 14th, 2021) for all lakes, as well as during the late season (March 27th, 2022) to capture the variability of snow depth in late season on a deeper snowpack on Landing Lake. Here, we will refer to Landing-D Lake to represent data collected in December and Landing-M Lake to represent data collected in March. The other three lakes will be referred to as Finger, Long and Vee Lakes. During

90   initial data collection, air temperatures ranged from -30°C to -15°C, and initial snow on the ground (December 7th, 2021) reported on land at the nearby Meteorological Service of Canada Yellowknife A weather station was 18 cm (Figure 2). During the time spent in the field, an additional 8 cm of snow fell (December 7 to 14th, 2021). Returning in March 2022, the initial snow on the ground was reported at 42 cm and air temperatures around -20°C.

The Cryosphere

Discussions

Open Access

EGU
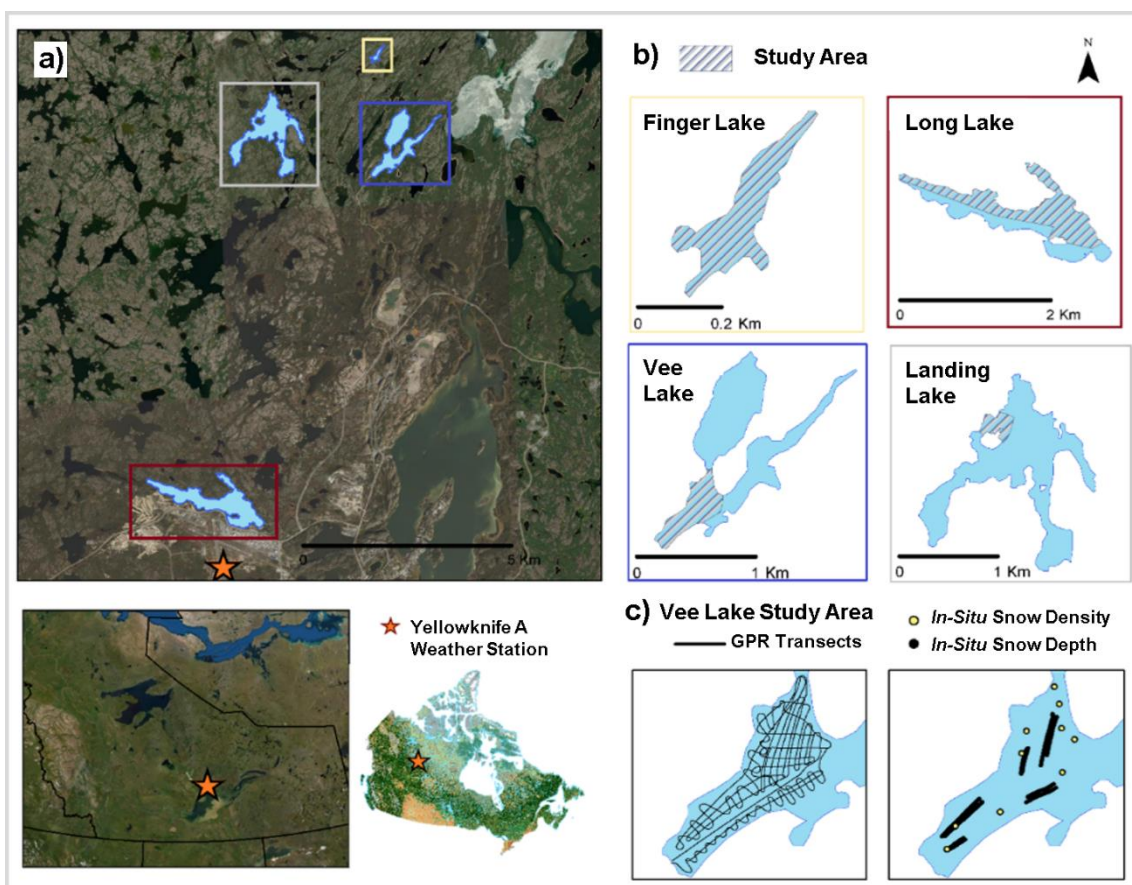
95

Figure 1: This study focuses on four lakes located north of Yellowknife, NWT, Canada, (b) Landing Lake, Finger Lake, Vee Lake, and Long Lake, shown on different scales depicting the area data collection took place (shaded colour). (c) The location of the GPR transects (Left) and in situ snow depth and density measurements (Right) on Vee Lake. (Background imagery: ESRI 2022, Landcover source: CCRS and NRCan, 2020)

100 **Table 1: Data collection occured on four lakes during early winter (December 2021) and late winter (March 2022, Landing Lake only) season. The surface area (SA), perimeter (P) and SA/P ratio are reported based on the entire shape of the lakes.**

Site	Date Visited	Latitude	Longitude	SA (km^2)	P (km)	SA/ P (km)
Finger Lake	12/09/2021	62.5750	-114.3587	0.04	1.44	0.03
Long Lake	12/12/2021	62.4772	-114.4422	1.13	10.35	0.11
Vee Lake	12/14/2021	62.5555	-114.3502	0.70	8.63	0.08
Landing-D Lake	12/07/2021	62.5587	-114.4103	1.08	11.71	0.09
Landing-M Lake	03/27/2022					
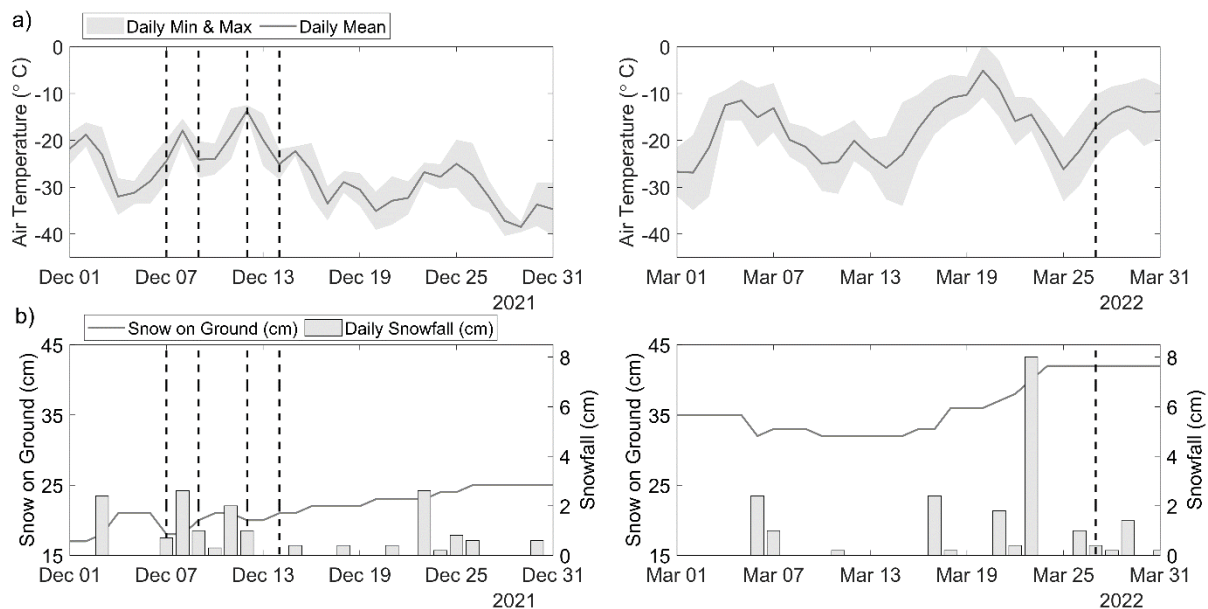
Figure 2: (a) The daily mean, minimum, and maximum air temperatures, and (b) snowfall and snow on the ground collected at the Yellowknife weather station are shown for each day spent in the field (dash line).

3 Methodology

3.1 GPR data acquisitions

GPR transects were acquired using the IceMap system (Sensors and Software Inc, 2022) paired with the 1000MHz Noggin sensor, with both the transmitting and receiving antennas oriented parallel at a fixed separation of 7.5cm. The IceMap system is configured with a GPS capable of recording location data simultaneously with the radar pulses, providing an accuracy of $\pm < 2$ m for the horizontal position. During the data acquisition, the IceMap GPR was set up in a sled pulled by a snowmachine. In the sled (Figure 3), the 1000MHz Noggin Sensor was positioned behind the IceMap box and lined up with a Leica Global Navigation Satellite System (GNSS) Real-Time Kinematic (RTK) rover (Leica Geosystems, 2018). Using the GNSS RTK rover, the location data was recorded at a higher accuracy, which was later processed and paired with the GPR pulse locations. This process improved the coordinate accuracy in 3-dimensions to $\pm < 0.02$ m (see Sect. 3.3.2). While traveling at ~ 4 m/s, the resulting GPR trace spacing was ~ 9 cm, dependent on any slight changes in the speed of the snowmachine. Approximately 38 km of GPR data was acquired over the four lakes initially traversed between December 7th to 14th, 2021 and an additional 6 km in March 2022, when revisiting Landing Lake. The transects were created following a gridded pattern to best cover the study area.
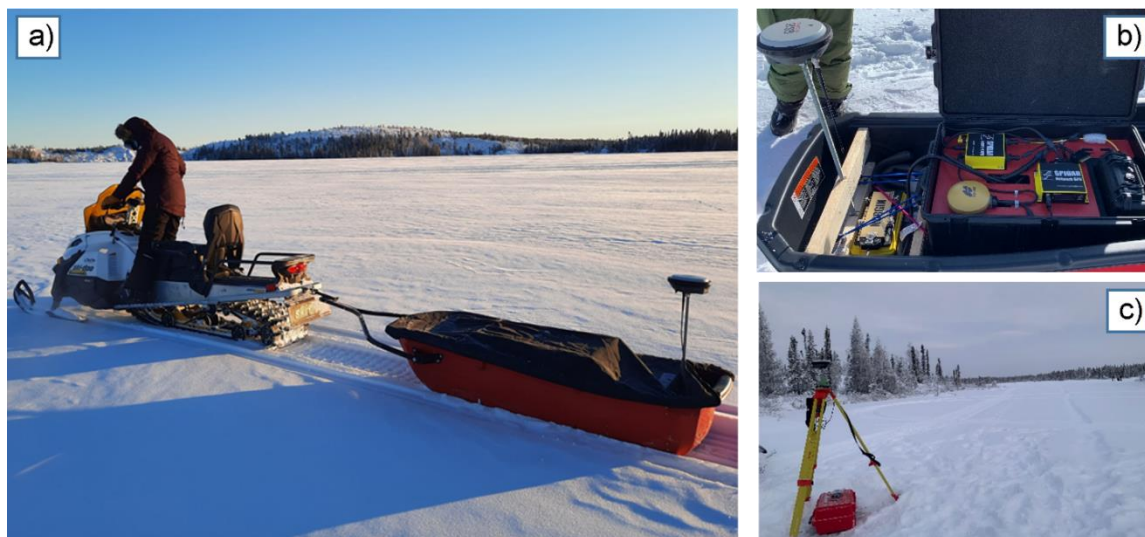
Figure 3: (a) The GPR was pulled by a snowmachine. (b) The 1000 MHz sensor was paired with the GPR and an external GNSS rover recorded data simultaneously, to improve the spatial accuracy of the collected transects. (c) A local base station was set up on the lake for GNSS post-processing.

3.2 In situ observations

In situ snow depth and density observations were gathered across areas of undisturbed snow and close to the GPR transects, as shown in Figure 1c. Snow depths (Table 2) were collected using a SnowHydro Magnaprobe (Sturm et al., 1999; SnowHydro, 2013) along grids or transects across the lake, with the average spacing varying between lakes (~ 2.5 m). The magnaprobe is equipped with a metal rod probe that penetrates the snowpack to the ice surface and a sliding basket that sits on the surface of the snow, recording the snow depth. The spatial accuracy for the magnaprobe GNSS receiver with use in the Arctic has been reported as ± 5 to10 m (Walker et al., 2020), with a 0.01 m depth precision (Sturm and Holmgren, 2018). With known limitations in the Magnaprobe GNSS accuracy, we used the RTK GNSS rover to measure the location of 291 magnaprobe measurements spaced out along the sampling transects on three of the four lakes (Landing, Finger, Vee). We found the error from the magnaprobe GNSS to be between 1.72 m to 8.43 m, with a mean (± standard deviation) error of 4.44 ±1 m.

For each lake, snow density was sampled at 6 to 10 locations which were then averaged (Table 2). The mean snow density is used as a guide in determining the appropriate density to use in deriving the snow depth. With limitations in fully capturing the variability of density across each area of focus, in later steps (see Sect. 3.3.4), we applied densities within ±1 standard deviation of the mean to derive the snow depth from the GPR TWT.

Table 2: In situ snow depth, h_s and density, ρ measurements were taken on the four lakes in December 2021 and, March 2022 on Landing-M. The density and snow depth varied between the four lakes (r = range, σ = standard deviation, n = count).

Site			Mean	Min	Max	r	σ	n
Finger Lake	$ρ$	kg/m^3	160	140	190	50	15	10
	h_s	cm	13.52	4.84	18.48	13.54	2.73	583
Long Lake	$ρ$	kg/m^3	245	180	310	130	47	7
	h_s	cm	13.98	6.12	23.78	17.66	3.29	475
Vee Lake	$ρ$	kg/m^3	195	160	270	90	34	8
	h_s	cm	16.09	6.29	21.00	14.71	2.48	427
Landing-D Lake	$ρ$	kg/m^3	170	140	200	60	21	6
	h_s	cm	10.21	4.34	18.89	14.55	2.33	617
Landing-M Lake	$ρ$	kg/m^3	220	182	300	118	36	10
	h_s	cm	35.61	24.70	50.81	26.02	4.54	595

3.3 Snow depth retrievals for GPR data

3.3.1 GPR signal processing

The snow-ice interface is challenging to identify due to interference between the direct wave and the reflection from the shallow snow-ice interface, in addition to the noise caused by wavefield scattering and antenna bounce. To account for this, signal processing was applied to the radargrams to remove any noise before automatically picking the TWTs. Initial processing consisted of applying a de-WOW filter (band-pass filter with a mean subtraction) to the measured amplitudes for each trace (Gerlitz et al., 1993). Next, a time-zero correction was applied to correct the first break times to ensure the snow surface was set to zero nanoseconds (Ihamouten et al., 2010). Followed by a background median subtraction filter, which removed the coherent "ringing" noise and the direct arrivals that masked the shallow reflections (Kim et al., 2007). Additionally, trace stacking was applied to smooth the image (Yilmaz, 2001).

3.3.2 GPR trace location correction

Through simultaneously collecting spatial data using the RTK rover during the GPR data acquisition, the timestamps from both the RTK GNSS and GPR GPS were used to pair the points and replace the spatial data of the GPR with the location recorded from the RTK GNSS. The RTK GNSS spatial data (X, Y, Z) was set to collect every 0.5 m for each lake. To account for the lower collection frequency of the RTK rover, the GPR traces that were not paired with an RTK GNSS point were linearly interpolated. In comparing the accuracy of the GPR GPS to the RTK GNSS for the paired locations, the error in GPS accuracy (easting & northing) was between 0.22 m to 4.97 m, with a mean Euclidean difference of 2.63 ± 1.21 m.

The Cryosphere
Discussions

3.3.3 Automatically picking GPR TWT

The GPR TWTs were extracted using the modified energy ratio algorithm (Wong et al., 2009), which automatically picks the first break. With the input of an estimated depth and wave speed, the picker is guided to a region of the time window and picks
160   the first initial zero crossing of the wavelet reflection, identifying the TWT. The radargram after signal processing can be seen in Figure 4a showing the TWT automatic picks along a transect on Landing-D Lake. Viewing Figure 4b as a function of elevation (meters above sea level), the variation in snow surface and thickness as well as ice surface can be seen.
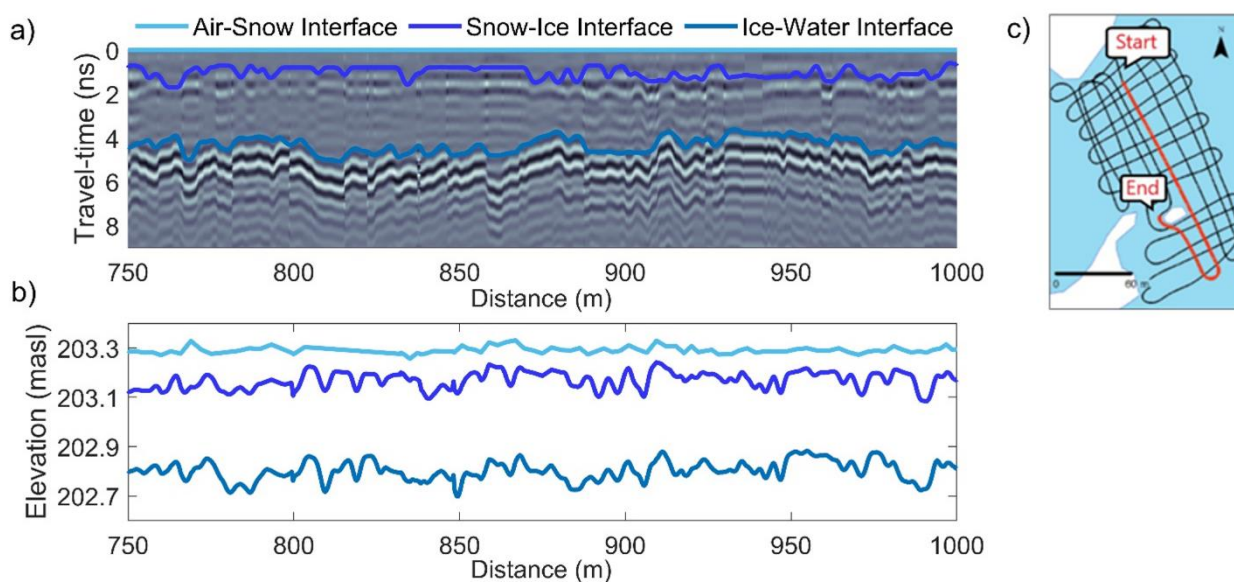
Figure 4:(a) After applying signal processing, the modified energy ratio algorithm was used to automatically pick the TWTs. The
165   air-snow interface is represented at time-zero and the snow-ice and ice-water interfaces were picked using the first initial zero crossing of the wavelet reflection. (b) The automatic TWT picks are shown as a function of elevation, where the variability in snow surface, ice surface, and the ice bottom can be seen. (c) The location for this 250 m example is on Landing-D Lake.

3.3.4 Calculating snow depth from TWTs and density

Snow depth was derived using the automatically picked TWTs and the wave speed of the radar signal. To determine the wave
170   speed of the radar signal traveling through the snow, the Kovacs et al. (1995) method of calculating the relative permittivity was used. The measured in situ snow density within a range of one standard deviation of the average for each lake (Finger = 175 kg/m^3, Long = 245 kg/m^3, Vee = 195 kg/m^3, Landing-D = 190 kg/m^3, Landing -M = 200 kg/m^3) was used to calculate relative permittivity using Eq. (1) as:

$$\varepsilon_r = (1 + 0.845\rho)^2 \tag{1}$$

175 where ρ is the density of snow, ε_r is the relative permittivity. As the speed of wave (V) at which the EM wave moves through snow depends on the snow relative permittivity, V was calculated using Eq. (2) as:

$$V = \frac{C}{\sqrt{\varepsilon_r}} \tag{2}$$

where C is the speed of light (0.3 m/ns) and ε_r is the relative permittivity. V is calculated for each lake (Finger = 0.261 m/ns, Long = 0.249 m/ns, Vee =0.258 m/ns, Landing-D = 0.259 m/ns, Landing-M =0.257 m/ns) and therefore, snow depth (h_s) was

180 derived using Eq. (3) as:

$$h_s = \frac{V \times TWT}{2} \tag{3}$$

where TWT is the two-way GPR travel-time.

3.4 Comparing GPR TWT derived snow depth to in situ snow depth

Derived snow depths from GPR TWTs were compared to in situ snow depth measurements collected during fieldwork. Around

185 each measured in situ snow depth, the GPR traces that fell within a 6 m radius were used to compare the accuracy of the derived snow depth. The 6 m radius was chosen due to the location accuracy calculated with the in situ snow depth observations (mean error of 4.44 ±1 m; see Sect. 2.4.2). The snow depths were derived in two different scenarios: 1) *closest match*, where the single closest matched snow depths within the 6 m radius was selected, 2) *distance weighting,* where the closest 50 % of total matched snow depths within the 6 m radius were selected and distance weighted. The removal of 50 % minimizes the

190 selection of GPR traces over the 6 m span and accounts for the spatial variability in snow depth expected over this 6 m length scale.

4 Results

4.1 Snow depth from GPR TWT

Collected GPR data across the four lakes traversed in December 2021 resulted in 406,164 derived snow depth observations

195 (Figure 5). The GPR-derived snow depths ranged from ~ 7 cm to 25 cm (Table 3), with the shallowest mean snow depth observed on Landing-D Lake on December 7th at 12.76 ± 3.25 cm, and the deepest mean snow depth on Vee Lake on December 14th by 16.06 ± 3.08 cm. The GPR transects on Landing-D Lake covered the smallest area of focus relative to the size of the lake (2.5%) and distance traversed (~ 3 km) and showed snow depth variability of 15 cm around islands, open areas, and shorelines. The entirety of Finger Lake (area = 4 ha) was traversed on December 9th, where deeper snow depths were observed

200 along shorelines and the closed-off areas (max = 24.83 cm), compared to the open stretch of the lake (min = 6.53 cm). Collected snow depth data on Long Lake on December 12th showed the largest spatial area, spanning 3 km from northwest to southeast,

with a total distance covered of 16 km. Long Lake showed the largest range in snow depth (6.21 cm to 22.34 cm) and density (180 kg/m3 to 310 kg/m3).
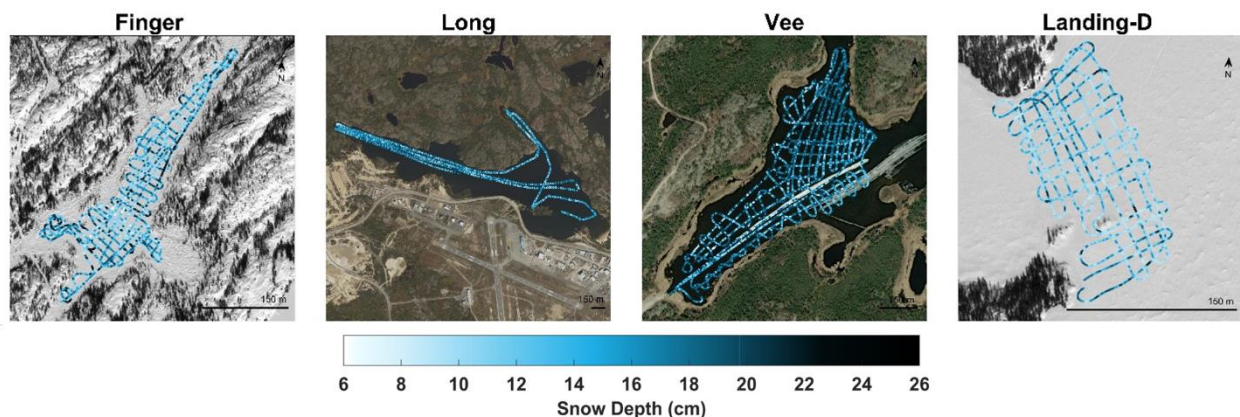
Figure 5: Maps show the 406,164 GPR-derived snow depth observations along the transects over each lake for December 2021. (Background imagery: ESRI 2022)

Table 3: The GPR TWT-derived snow depth statistics from the four lakes during the December 7– 14, 2021 (r = range, σ = standard deviation, n = count, d = distance traversed, and s = average trace spacing)

Site	Mean (*cm*)	Min (*cm*)	Max (*cm*)	r (*cm*)	σ (*cm*)	n	d (*km*)	s (*cm*)
Finger Lake	14.60	6.53	24.83	18.29	3.55	63589	5.36	0.08
Long Lake	14.68	6.21	22.34	16.13	3.29	152554	16.27	0.11
Vee Lake	16.06	6.44	23.18	16.74	3.08	151853	12.72	0.08
Landing-D Lake	12.76	7.60	22.42	14.67	3.25	38168	3.06	0.08

4.2 Comparing GPR vs. magnaprobe snow depths

The in situ snow depth observations (n =1932) were used for all four lakes to validate the GPR-derived snow depth in December 2021. The comparison of in situ and GPR-derived snow depths for scenarios 1 and 2 are shown in Figures 6 and 7. We found that the minimum error snow depth exists within a 6 m radius (R^2 = 0.92, RMSE = 0.74 cm, MAE = 0.26 cm on average) for all four lakes (Figure 6a). The distance of each minimum error pair was, on average, 3.79 ± 1.5 m apart, compared to the measured accuracy error with the magnaprobe (4.44 ± 1 m). Through identifying the distance between each GPR and in situ snow depth pair, we confirmed that the GPR measurements further away (within 6 m radius) from the in situ snow depth are the appropriate pairs in most cases (Figure 6b). Therefore, we applied scenario 2 to evaluate the accuracy of the GPR-derived snow depths (Table 4) and applied scenario 2 for further data analysis.
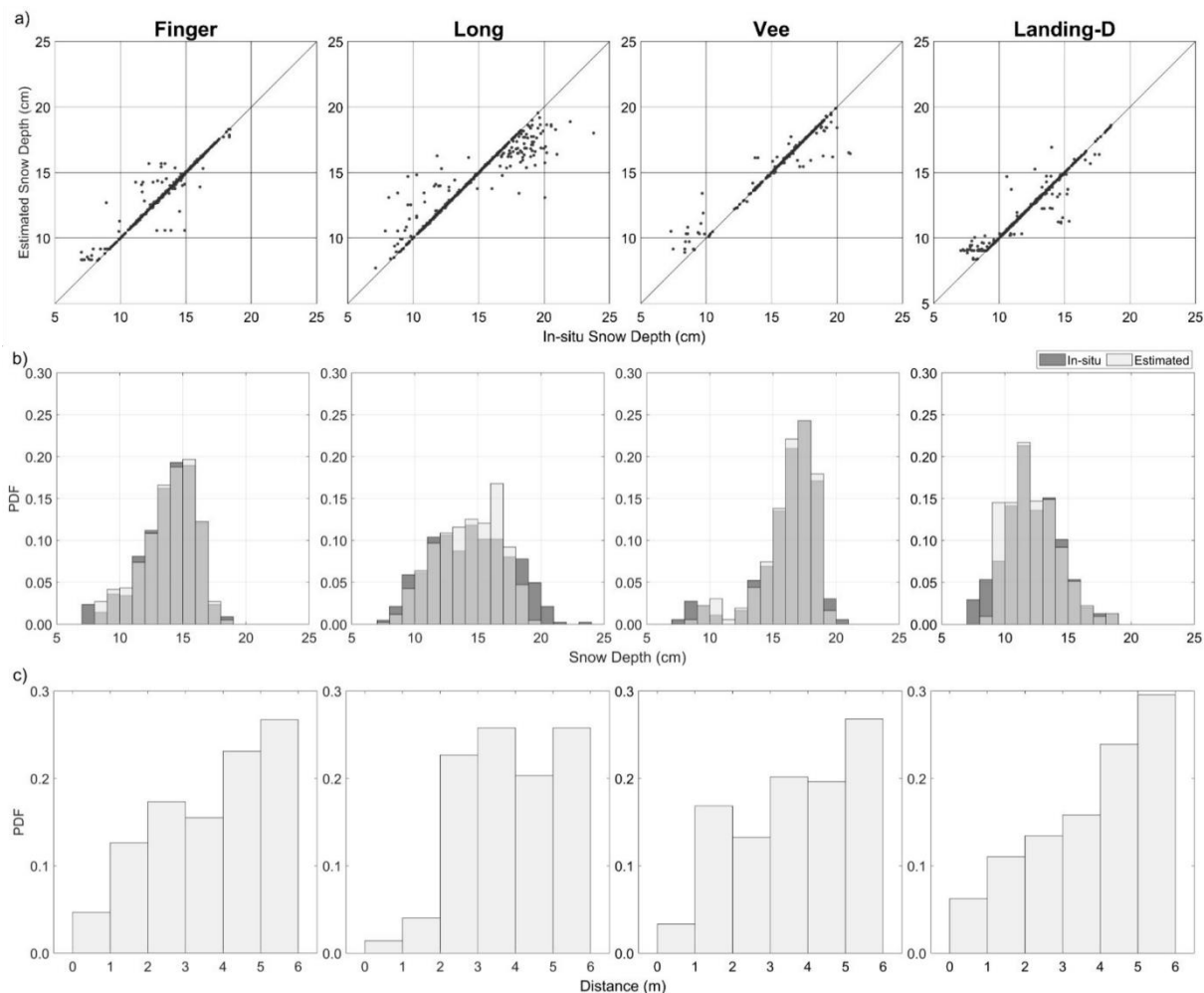
Figure 6: Validation of GPR-derived snow depths using a 6m radius, Scenario 1 *(closest match),* **(a) scatterplots and (b) histograms**
220 **of the in situ and GPR-derived snow depth, and (c) bar plots of the distance from the paired in situ to GPR-derived snow depth.**

Scenario 2 showed strong agreement between the in situ and estimated observations (Figure 7) with $R^2 = 0.63$, RMSE = 1.58
and MBE = 1.05 cm on average for all lakes. Long Lake showed the lowest agreement ($R^2 = 0.50$, RMSE = 2.19 cm, MAE =
1.52 cm) with the GPR-derived snow depth showing slight over and under estimations. The strongest agreement was found on
Vee Lake with $R^2 = 0.71$, RMSE = 1.40 cm, and MAE = 0.83 cm. The relative error of the GPR-derived snow depth was 8.22
225 % on average for all four lakes traversed in December, with Vee Lake being the most accurate (relative error = 6.25 %) and
Long Lake the least (relative error = 11.04 %).
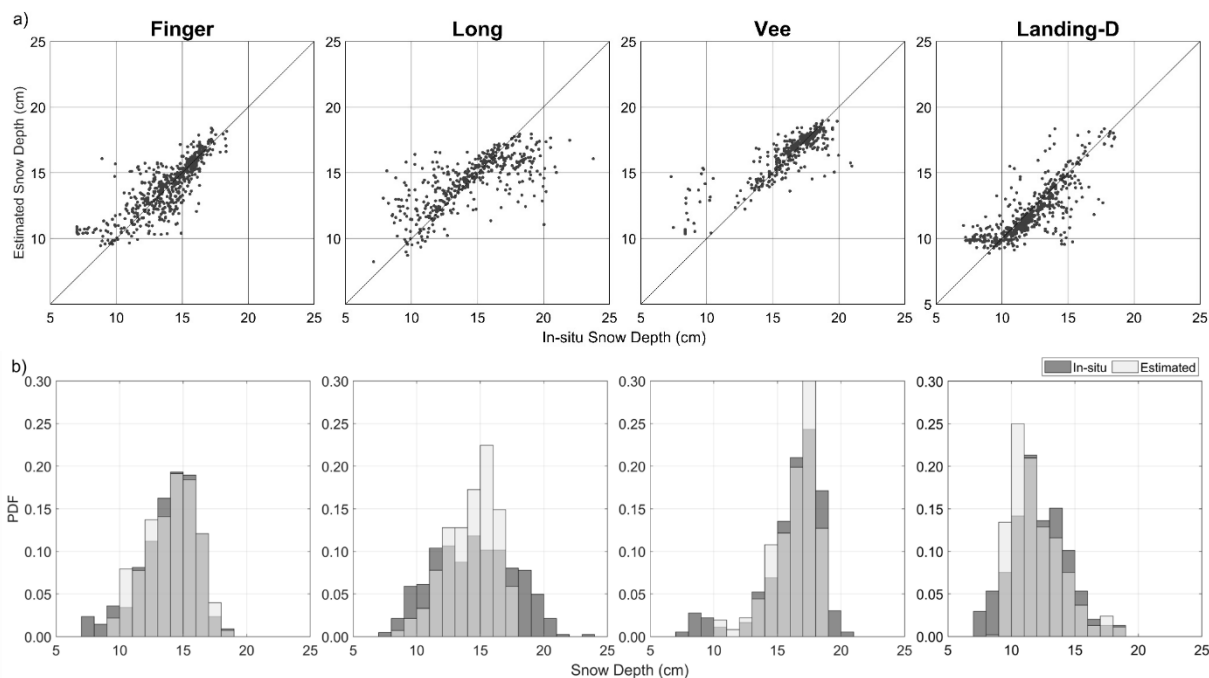
Figure 7: Validation of GPR-derived snow depths using a 6m radius, Scenario 1 (*Distance weighting*), (a) scatterplots, and (b) histogram of the in situ and GPR-derived snow depth.

230 **Table 4: Statistics of GPR derived snow depths versus the magnaprobe collected snow depths for Scenario 2.**

Site	R^2	MAE (*cm*)	RMSE (*cm*)	Bias (*cm*)	Relative Error (%)	n
Finger	0.66	0.92	1.33	-0.14	7.52	554
Long	0.50	1.52	2.19	0.13	11.04	472
Vee	0.71	0.83	1.40	-0.20	6.33	362
Landing-D	0.63	0.94	1.38	0.16	8.06	544
Mean	**0.63**	**1.05**	**1.58**	**-0.01**	**8.24**	

4.3 Early season vs. late season

Landing Lake was revisited for the data collection on March 27th, 2022, resulting in an additional 73,732 snow depth observations from GPR TWTs over ~ 6 km (Figure 8). In December 2021 and March 2022, the snow depth derived on Landing Lake varied, with Landing-D Lake ranging from ~ 8 to 22.50 cm and Landing-M Lake from ~ 10 to 50 cm. The snow depth
235 was, on average, 12.76 (± 3.25) cm in December and more than twice that in March (35.83 ± 2.54 cm). The snow density in the early season was, on average, 170 kg/m^3, whereas in the later season measured at an average of 220 kg/m^3 (Table 2). The results showed that agreement between in situ snow depth observations and Landing-M Lake GPR-derived snow depth (R^2 = 0.66, RMSE = 2.86 cm, Bias = 0.41 cm, n = 498) was not significantly improved when compared with Landing-D Lake (Figure 8). However, the relative error was improved on Landing-M Lake with a deeper snowpack (5.33 %) than that of Landing-D

Lake (8.06 %). During the later season, the GPR could derive the minimum snow depths seen on Landing Lake, as opposed to
that in the early season, where the GPR-derived snow depth could not capture the shallowest snow area (4.5 - 10 cm).
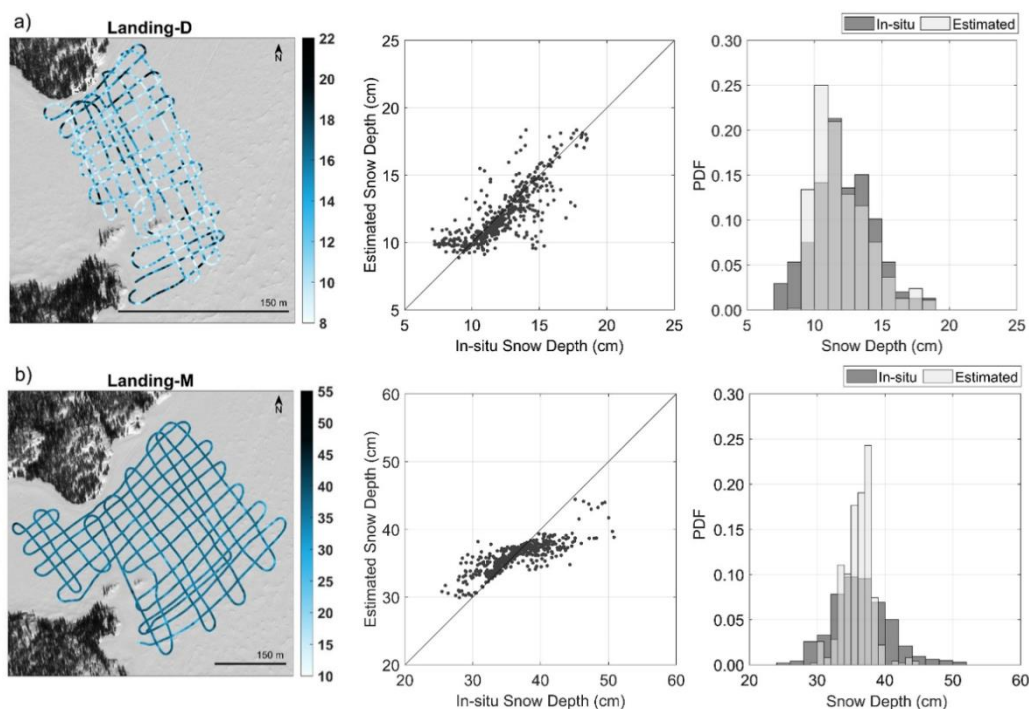
Figure 8: Maps show the GPR derived snow depth on GPR transects and the scatterplot and bar plot compare in-situ data vs GPR-derived snow on (a) Landing-D Lake during December 2021 and (b) Landing-M Lake during March 2022 (Background imagery: ESRI 2022)

4.4 Snow depth mapping

Snow depth distribution maps were generated at a 1 m resolution through interpolating (inverse-distance weighting) the GPR-derived snow depth observations (Figure 9). Through re-gridding to 1 m resolution and interpolating, the snow depths ranged from 8 cm to 22 cm in December 2021. The deepest snowpack, on average, was observed on Vee Lake (15.99 ± 0.79 cm), ~ 4 cm deeper than Landing-D Lake (12.73 ± 0.87 cm) during December 2021 field campaign. The interpolated GPR-snow depths consistently show deeper snow around the shoreline perimeter and catchment areas and shallower snow on the open areas. Transect profiles (Figure 9) created over the 1 m resolution snow depth maps show an example of the variability in snow depth across each lake. The spatial correlations of the 1 m resolution snow depths from the GPR transects were estimated using an experimental semi-variogram that was fit using an exponential model for December 2021 and March 2022 data collected (Figure 10). The largest correlation length was observed on Landing-M Lake (18.18 m). The correlation length on Landing-D

13

Lake in the early season was measured at ~10 m less than that of the late winter season, while Long Lake showed the smallest distance, at 6.42m over the largest spatial area.
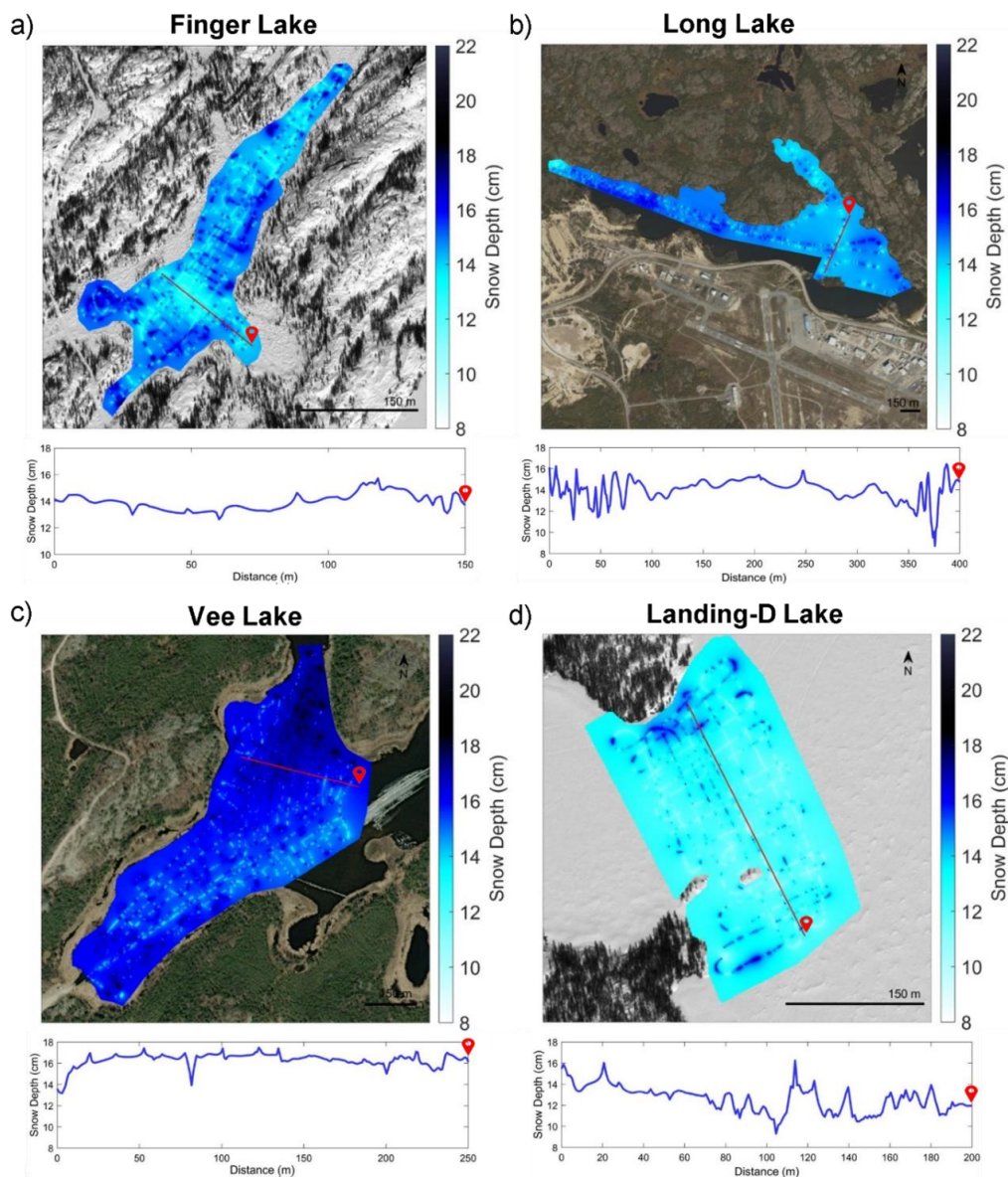
Figure 9: Maps show the GPR-derived snow depth using an inverse-distance weighted model to interpolate the snow depth over (a) Finger Lake, (b) Long Lake, (c) Vee Lake, (d) Landing-M Lake at 1 m resolution and showing a transect profile across a portion of the lake (profile transect ends at the red symbol marked on each lake)(Background imagery: ESRI 2022).
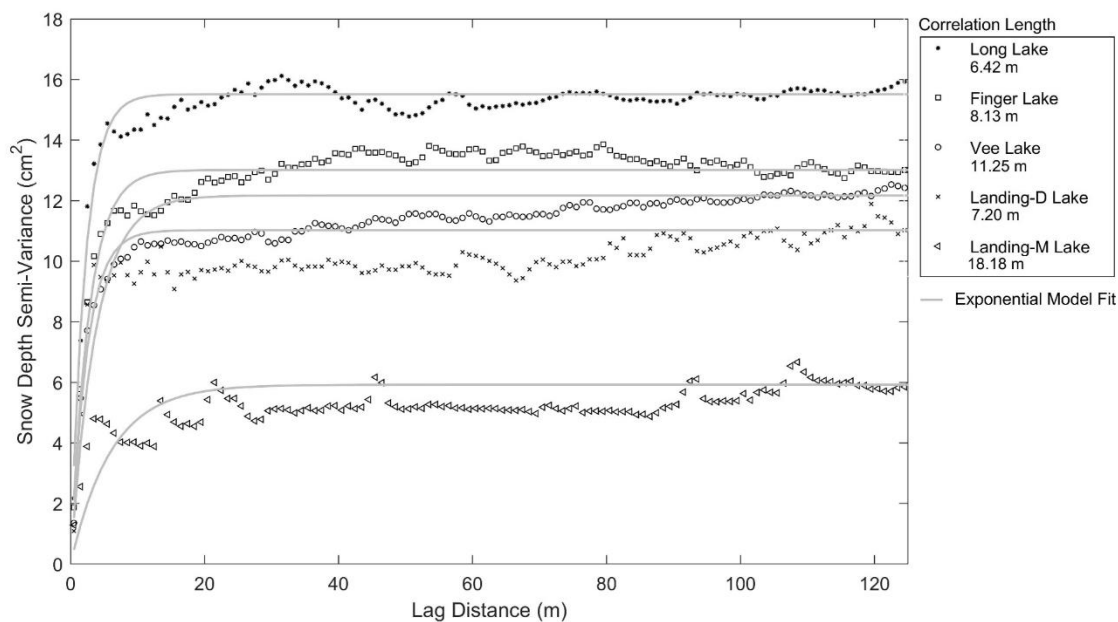
Figure 10: The experimental variograms for GPR-derived snow depth transects were fit to an exponential model to determine the correlation length.

5 Discussion

This study develops our ability to collect snow depth observations over large areas of lakes accurately and efficiently, which are comparable with previous studies using GPR TWT over land and sea ice (Pfaffhuber et al., 2017; McGrath et al., 2019). While GPR has been utilized to retrieve seasonal snowpacks over land and sea ice, this study reveals the success GPR can have in deriving snow depth over lake ice, where the snowpack is generally shallow and the snow-ice interface is challenging to capture (Sturm and Liston, 2003). In December 2021 and March 2022, the lakes consistently showed a shallower snowpack on average (Table 3) than snow on the ground (Figure 2) reported at the nearby Yellowknife weather station (an average of 24 to 29 % less than snow over land in December 2021, and 15 % less in March 2022). This confirms that applying snow depths measured on land as an input to lake ice models to represent snow over lake ice will impact the model accuracy due to overestimating the snow depth. Additionally, this study demonstrated the distribution of snow over each lake (Figure 9), which showed local-scale variability of snow depths from redistribution of the snow across all the lakes (correlation lengths between 6 – 19 m). These lengths are similarly supported in the literature, reporting correlation lengths from 5 to 20 m (Gunn et al., 2021a; Sturm and Liston, 2003), as the snow distribution over lake ice is known to be affected by wind and surrounding vegetation (Adams, 1976a). We found Long Lake to have the shortest correlation length (6.42 m) and the largest surface area to perimeter ratio. The northwest to the southeast extent for Long Lake is ~3 km and is likely more exposed to wind

15

280 redistribution. Moreover, the lower accuracy found on Long Lake could be attributed to using a 6 m radius to compare the estimated and in situ snow depth, as snow distribution was found to vary at the same length scale.

During the field campaign, we used both the 1000 MHz and 500MHz GPR antennas; however, we have found that 1000 MHz can estimate shallow snow more accurately, especially during the early-season, due to the shorter wavelength (not shown). Overall, the results of this study showed that a 7 cm threshold exists as a limitation of deriving shallow snow depth from GPR

285 TWT using the 1000 MHz sensor. Showing similar agreement with previous studies (Pfaffhuber et al., 2017), the in situ observations below 7 cm were not considered in the validation analysis. On Landing-D Lake, there was frequent snow depression of the magnaprobe basket (~2 cm on average), where it sat below the snow surface. To account for the depression of the magnaprobe basket, we have corrected the in situ data for Landing-D Lake by 2 cm. We have found that no correction is needed for compaction caused by the GPR sled, as we found that the sensitivity in snow depth due to snow density was

290 minor for shallow snowpacks. Therefore, the retrieved snow depth was minimally affected by spatial density variability. The snow density proved 0.16 to 0.50 cm of uncertainty with the GPR-derived snow depth in December 2021 and 0.90 cm in March 2022, based on the mean and ± 1 standard deviation measured in the field. Although there is a change in density on the sled track ($\bar{\rho}_{sled}$ = 340 ± 20 kg/m^3) compared to the density of the fresh snow (Table 2), the effects of a decrease in depth and increase in density under compaction from the snowmachine are naturally compensated. Therefore, the effect on GPR derived

295 snow depth is minimal because minimal snow mass was lost. The snow depth was measured to be, on average, 1.5 cm less by using the density of the sled track for depth estimation rather than fresh snow density. Snow density is known to vary spatially in three-dimension (King et al., 2020), but this was not well represented in this study. The effect of snow density on lake ice formation needs to be further investigated, however, we found that this effect on snow depth retrieval was minimal due to the shallow nature of snow on the lake ice, thus permitting the use of a constant density in deriving shallow snow depth from GPR.

6 Conclusion

300

We applied an automated processing method to derive snow depth over lake ice accurately and efficiently using 1000 MHz GPR acquisitions. The radar wave speed was derived and applied as a constant from the snow density measured on each lake to convert the GPR TWTs to snow depth. The GPR traces were collected more efficiently than manual snow observations, covered a larger spatial area, and required minimal time in the field. Additionally, GPR-derived snow depths were collected at

305 a higher spatial resolution (mean GPR sample distance ~ 0.09 m, mean magnaprobe sample distance ~ 2.5 m). Therefore, it can identify the spatial variability of snow depth across lake ice over a larger spatial area, which can make it possible to explore the effects of wind redistribution and shoreline vegetation. We collected ~ 500,000 GPR-derived snow depth observations during the five days spent in the field.

The snow depths derived using GPR TWT over lake ice show similar accuracies compared to studies that use comparable

310 methods over land and sea ice, with a relative error under 10 %. The GPR can measure shallow snowpacks over lake ice in the

The Cryosphere
Discussions

Open Access

EGU

early and late winter seasons. The continuous point measurements at a high spatial resolution allow interpolating the snow depth to map the snow on the lake. The results provide large, accurate data sets that can benefit the modelling community and significantly improve thermodynamic lake ice modelling.

Code and data availability

315   Data will be available through the Government of Northwest Territories' Discovery Portal (GNWT Discovery Portal) as well as ReSEC Lab data portal - **DOI (will be replaced after review process with public DOI)**. This manuscript is a slightly modified version of AP master thesis (Pouw, 2023).

Author contributions

AP: Methodology design, Data collection, Data processing, analysis, & visualization, Writing –original draft. HP: Supervision,
320   Resources, Methodology design, Data collection, Writing –editing original draft. AM: Methodology design, Data collection, Writing –editing original draft.

Competing interests

Some authors are members of the editorial board of *The Cryosphere*. The peer-review process was guided by an independent editor, and the authors have also no other competing interests to declare.

The Cryosphere
Discussions
Open Access
EGU

References

335   Adams, W.P.: Diversity of lake cover and its implications. Musk-Ox, 181, 86–98, 1976a.

Adams W.P.: A classification of freshwater ice. Musk-Ox, 18, 99–102, 1976b.

Barrette, P.D.: The Tibbitt to Contwoyto winter road in the NWT:identification of available data and research needs. NRC
    Publications Archive. National Research Council of Canada. Canadian Hydraulics Centre. No. CHC-LM-006, doi:
    10.4224/40000399, 2011.

340   Benson, B. J., Magnuson, J. J., Jensen, O. P., Card, V. M., Hodgkins, G., Korhonen, J., Livingstone, D. M., Stewart, K. M.,
    Weyhenmeyer, G. A., and Granin, N. G.: Extreme events, trends, and variability in Northern Hemisphere Lake-ice
    phenology (1855–2005). Climatic Change, 112, 299–323, doi:10.1007/s10584-011-0212-8, 2011.

Brown, L. C. and Duguay, C. R.: The response and role of ice cover in lake-climate interactions. Prog. Phys Geog., 34, 671-
    704, doi:10.1177/0309133310375653, 2010.

345   Brown, L. C., and Duguay, C. R.: The fate of lake ice in the North American Arctic. The Cryosphere, 5, 869-892.
    doi:10.5194/tc-5-869-2011, 2011.

Brown, R. D., Smith, C., Derksen, C., and Mudryk, L.: Canadian in situ snow cover trends for 1955–2017 including an
    assessment of the impact of automation. Atmos. Ocean, 1–16, doi:10.1080/07055900.2021.1911781, 2021.

Canada Centre for Remote Sensing (CCRS) and Natural Resources Canada (NRCan). 2015 Land Cover of North America at
350   30 meters. *North American Land Change Monitoring System.* Ottawa, Ont. Data available: http://www.cec.org/north-
    american-environmental-atlas/land-cover-30m-2015-landsat-and-rapideye/ , 2020.

Gerlitz, K., Knoll, M. D., Cross, G. M., Luzitano, R. D., and Knight, R.: Processing Ground Penetrating Radar Data to Improve
    Resolution of Near Surface Targets. Symp. Appl. Geophys. to Eng. Environ. Probl. Environment and Engineering
    Geophysical Society, 561-574, doi:10.4133/1.2922036, 1993.

355   Gunn, G. E., Duguay, C. R., Brown, L. C., King, J., Atwood, D., and Kasurak, A.: Freshwater lake ice thickness derived using
    surface-based X- and ku-band FMCW scatterometers. Cold Reg. Sci. Technol., 120, 115–126. doi:
    10.1016/j.coldregions.2015.09.012, 2015.

Gunn, G. E., Jones, B. M. and Rangel, R. C.: Unpiloted Aerial Vehicle Retrieval of snow depth over freshwater lake ice using
    structure from Motion. Frontiers in Remote Sensing, 2, doi:10.3389/frsen.2021.675846, 2021a.

360   Gunn, G. E., Tarabara, V., Rutty, M., Bessette, D. L., and Richardson, R. B.: Roughness and storage capacity of freshwater
    ice in the straits of Mackinac. Cold Reg. Sci. Technol., 186, 103278. doi:10.1016/j.coldregions.2021.103278, 2021b.

Harder, P., Schirmer, M., Pomeroy, J., and Helgason, W.: Accuracy of snow depth estimation in mountain and prairie
    environments by an unmanned aerial vehicle. The Cryosphere, 10, 2559–2571, doi:10.5194/tc-10-2559-2016, 2016.

Harder, P., Pomeroy, J. W., and Helgason, W. D.: Improving sub-canopy snow depth mapping with unmanned aerial vehicles:
365   Lidar versus structure-from-motion techniques. The Cryosphere, 14, 1919–1935, doi:10.5194/tc-14-1919-2020,
    2020.

Ihamouten, A., Dérobert X., and Villain G.: The effect of coupling on the determination of time zero for radar antennae. *Proceedings of the XIII Internarional Conference on Ground Penetrating Radar*, doi:10.1109/icgpr.2010.5550082, 2010.

370   Jensen, O. P., Benson, B. J., Magnuson, J. J., Card, V. M., Futter, M. N., Soranno, P. A., and Stewart, K. M.: Spatial analysis of ice phenology trends across the Laurentian Great Lakes region during a recent warming period. Limnol. Oceanogr., 52, 2013–2026, doi:10.4319/lo.2007.52.5.2013, 2007.

Kheyrollah Pour, H., Duguay, C. R., Scott, K. A. and Kang, K.: Improvement of lake ice thickness retrieval from MODIS satellite data using a thermodynamic model. IEEE T. Geosci.Remote., 55, 5956-5965 doi:10.1109/tgrs.2017.2718533
375   , 2017.

Kholoptsev, A. V., Podporin, S. A., and Karetnikov, V. V.: Current trends in the ice thickness and concentration on the waterways of the Arctic. IOP Conference Series: Earth and Environmental Science, 867, 012013, doi:10.1088/1755-1315/867/1/012013, 2021.

Kim, J.H., Cho, S.J. and Yi, M.J.: Removal of ringing noise in GPR data by signal processing. Geosci. J., 11, 75-
380   81.doi:10.1007/BF02910382, 2007.

King, J., Howell, S., Brady, M., Toose, P., Derksen, C., Haas, C., and Beckers, J.: Local-scale variability of snow density on Arctic sea ice. The Cryosphere, 14, 4323-4339. doi:10.5194/tc-14-4323-2020, 2020.

King, F., Kelly, R., and Fletcher, C.G.: Evaluation of lidar-derived snow depth estimates from the iPhone 12 pro. IEEE Geosci. Remote Sens. Lett., 19, 1–5. doi:10.1109/lgrs.2022.3166665, 2022.

385   Knoll, L. B., Sharma, S., Denfeld, B. A., Flaim, G., Hori, Y., Magnuson, J. J., Straile, D., and Weyhenmeyer, G. A.: Consequences of lake and river ice loss on Cultural Ecosystem Services. Limnol. Oceanogr., 4, 119–131, doi:10.1002/lol2.10116, 2019.

Kovacs, A., Gow, A. J. and Morey, R. M.: The in-situ dielectric constant of polar firn revisited. Cold Reg. Sci. Technol., 23, 245-256, doi:10.1016/0165-232X(94)00016-Q , 1995.

390   Leica Geosystems.: Leica GS10. St. Gallen, Switzerland, 2018.

Leppäranta, M.: A growth model for black ice, snow-ice and snow thickness in subarctic basins. Nordic Hydrol., 14, 59–70, 1983.

Leppäranta, M.: Freezing of Lakes and the Evolution of their Ice Cover; Springer: Berlin/Heidelberg, Germany, 84–265, 2015.

395   Magnuson, J. J., Robertson, D. M., Benson, B. J., Wynne, R. H., Livingstone, D. M., Arai, T., Raymond, A.A., Barry, R.G., Card, V., Kuusito, E., Granin, N.G., Prowse, T.D., Stewart, K.M., and Vuglinski, V. S.: Historical Trends in Lake and River Ice Cover in the Northern Hemisphere. Science, 289, 1743 LP – 1746. doi:10.1126/science.289.5485.1743, 2000.

Marsh, C. B., Pomeroy, J. W., Spiteri, R. J., and Wheater, H. S.: A finite volume blowing snow model for use with variable
400   resolution meshes. Water Resour. Res., 56. doi:10.1029/2019wr025307, 2020.

Marshall, H., Koh, G., and Forster, R. R.: Estimating alpine snowpack properties using FMCW radar. Ann. Glaciol., 40, 157-162. doi:10.3189/172756405781813500 , 2005.

McGrath, D., Webb, R., Shean, D., Bonnell, R., Marshall, H. P., Painter, T. H., Molotch, N. P., Elder, K., Hiemstra, C. and Brucker, L.: Spatially extensive ground-penetrating radar snow depth observations during NASA's 2017 SnowEx campaign: Comparison with in-situ, airborne, and satellite observations. Water Resour. Res., 55, 10026–10036, doi:10.1029/2019wr024907, 2019.

McGrath, D., Bonnell, R., Zeller, L., Olsen-Mikitowicz, A., Bump, E., Webb, R., and Marshall, H.-P.: A time series of snow density and snow water equivalent observations derived from the integration of GPR and UAV SFM Observations. Frontiers Remote Sens., 3. doi:10.3389/frsen.2022.886747, 2022.

Meehan, T.G., Marshall, H.P., Deeb, E., McGrath, D., and Webb, R.: Automatic detection of the ground through snow cover using multi-polarization coherency. International Conference on Ground Penetrating Radar, 18,85-88, doi: 10.1190/gpr2020-023.1, 2020.

Meehan, T. G., Marshall, H. P., Bradford, J. H., Hawley, R. L., Overly, T. B., Lewis, G., Graeter, K., Osterberg, E., and McCarthy, F.: Reconstruction of Historical Surface Mass Balance, 1984-2017 from GreenTrACS Multi-Offset Ground-Penetrating Radar. J. Glaciol. 67, 219–228. doi:10.1017/jog.2020.91, 2021.

Mullan, D. J., Barr, I. D., Flood, R. P., Galloway, J. M., Newton, A. M., and Swindles, G. T.: Examining the viability of the world's busiest winter road to climate change using a process-based Lake Model. Bull. Am. Meteorol. Soc., 102, doi:10.1175/bams-d-20-0168.1, 2021.

Pfaffhuber, A. A., Lieser, J. L., and Hass, C.: Snow thickness profiling on Antarctic sea ice with GPR— Rapid and accurate measurements with the potential to upscale needles to a haystack. Geophys. Res. Lett., 44, 7836-7844, doi:10.1002/2017GL074202, 2017.

Pouw, A. F.: Utilizing Ground-Penetrating Radar to Estimate the Spatial Distribution of Snow Depth over Lake Ice in Canada's Sub-Arctic, *Theses and Dissertations (Comprehensive)*, 2510, https://scholars.wlu.ca/etd/2510, 2023.

Robinson, A. L., Ariano, S. S., and Brown, L. C.: The Influence of Snow and Ice Albedo towards Improved Lake Ice Simulations. Hydrology, 8, 11. doi:10.3390/hydrology8010011, 2021.

Sensors & Software.: IceMap:Real-time, high-accuracy ice thickness measurements. [WWW Document]. Available from https://www.sensoft.ca/wp-content/uploads/2022/01/Icemap-Brochure_2022.pdf, 2022.

SnowHydro.: GPS snow depth probe [WWW Document]. Available from http://www.snowhydro.com/products/column2.html, 2013.

Stephenson, S.R., Smith, L.C., and Agnew, J.A.: Divergent long-term trajectories of human access to the Arctic. Nature Climate Change, 1, 156–160. doi:10.1038/nclimate1120, 2011.

Sturm, M., Holmgren, J., and Liston, G.E.: Self-recording snow depth probe. 1741, 1999.

Sturm, M. and Liston, G. E.: The snow cover on lakes of the Arctic Coastal Plain of Alaska, U.S.A. J. Glaciol., 49, 370–380. doi: 10.3189/172756503781830539, 2003.

435   Sturm, M., & Holmgren, J.: An automatic snow depth probe for field validation campaigns. Water Resour. Res., 54, 9695–
             9701. doi:10.1029/2018wr023559, 2018.

Walker, B., Wilcox, E. J. and Marsh, P.: Accuracy assessment of late winter snow depth mapping for tundra environments
             using structure-from-motion photogrammetry. Arctic Science, 7, 588–604, doi:10.1139/as-2020-0006, 2020.

Webb, R. W.: Using ground penetrating radar to assess the variability of snow water equivalent and melt in a mixed canopy
440   forest, Northern Colorado. Frontiers Earth Sci., 11, 482–495. doi:10.1007/s11707-017-0645-0, 2017.

Webb, R. W., Jennings, K. S., Fend, M., and Molotch, N. P.: Combining ground-penetrating radar with terrestrial lidar scanning
             to estimate the spatial distribution of liquid water content in seasonal snowpacks. Water Resour. Res., 54, doi:
             10.1029/2018wr022680, 2018.

Wong, J., Han, L., Bancroft, J. C. and Stewart, R. R.: Automatic time-picking of first arrivals on noisy microseismic data.
445   CREWS, 1–6, 2009.

Yilmaz, Ö.: Seismic Data Analysis. SEG. doi:10.1190/1.9781560801580, 2001.

Zhang, X., Flato, G., Kirchmeier-Young, M., Vincent, L., Wan, H., Wang, X., Rong, R., Fyfe, J., Li, G., Kharin, V.V.: Changes
             in Temperature and Precipitation Across Canada; Chapter 4 in Bush, E. and Lemmen, D.S. (Eds.) Canada's Changing
             Climate Report. Government of Canada, Ottawa, Ontario, pp 112-193, 2019.